Intranasal Administration of aTf Protects and Repairs the Neonatal White Matter After a Cerebral Hypoxic–Ischemic Event

MARIANO GUARDIA CLAUSI,[1] PABLO M. PAEZ,[2] ANTHONY T. CAMPAGNONI,[2] LAURA A. PASQUINI,[1] AND JUANA M. PASQUINI[1]*

[1]*Department of Biological Chemistry, School of Pharmacy and Biochemistry, and Institute of Chemistry and Biological Physicochemistry (IQUIFIB), School of Pharmacy and Biochemistry, University of Buenos Aires and National Research Council (CONICET), Argentina*

[2]*Semel Institute for Neuroscience and Human Behavior, Department of Psychiatry and Behavioral Sciences, David Geffen School of Medicine at UCLA, Los Angeles, California*

KEY WORDS
apotransferrin; hypoxia-ischemia; myelination; apoptosis; oligodendrogenesis

ABSTRACT
Our previous studies showed that the intracerebral injection of apotransferrin (aTf) attenuates white matter damage and accelerates the remyelination process in a neonatal rat model of cerebral hypoxia-ischemia (HI) injury. However, the intracerebral injection of aTf might not be practical for clinical treatments. Therefore, the development of less invasive techniques capable of delivering aTf to the central nervous system would clearly aid in its effective clinical use. In this work, we have determined whether intranasal (iN) administration of human aTf provides neuroprotection to the neonatal mouse brain following a cerebral hypoxic–ischemic event. Apotransferrin was infused into the naris of neonatal mice and the HI insult was induced by right common carotid artery ligation followed by exposure to low oxygen concentration. Our results showed that aTf was successfully delivered into the neonatal HI brain and detected in the olfactory bulb, forebrain and posterior brain 30 min after inhalation. This treatment successfully reduced white matter damage, neuronal loss and astrogliosis in different brain regions and enhanced the proliferation and survival of oligodendroglial progenitor cells (OPCs) in the subventricular zone and *corpus callosum* (CC). Additionally, using an *in vitro* hypoxic model, we demonstrated that aTf prevents oligodendrocyte progenitor cell death by promoting their differentiation. In summary, these data suggest that iN administration of aTf has the potential to be used for clinical treatment to protect myelin and to induce remyelination in demyelinating hypoxic–ischemic events in the neonatal brain.

INTRODUCTION

Earlier studies from our lab clearly show that apotransferrin (aTf) contributes to the differentiation and maturation of oligodendrocyte progenitor cells (OPCs). We have demonstrated that this glycoprotein is necessary at multiple stages during OPC development including OPC proliferation, migration, and differentiation (Guardia Clausi et al., 2010; Paez et al., 2002, 2004, 2005). Moreover, exogenous aTf has been shown to protect the brain against demyelination when injected directly into the central nervous system (CNS) (Adamo et al., 2006; Badaracco et al., 2008). In our most recent paper, we provided direct evidence that an intracerebral injection of aTf attenuated white matter damage in a neonatal rat model of cerebral hypoxia–ischemia (HI) injury (Guardia Clausi et al., 2010). However, the intracerebral injection of aTf might not be practical for clinical purposes. Therefore, the development of less invasive techniques capable of delivering aTf to the CNS would clearly aid in its effective clinical use.

A promising way to deliver drugs to the brain is the nasal route. The olfactory region is the only site of the body where the CNS is somehow in contact with the external environment, due to the presence of the olfactory receptor neurons, whose axons end in the olfactory bulb. Hence, a drug administered into the nasal cavity and deposited on the olfactory mucosa should have a good chance to reach the cerebrospinal fluid, upon diffusion across the mucosa itself. Afterward, the drug could diffuse into the interstitial fluid and reach the olfactory and/or trigeminal nerve pathways, or the vascular and lymphatic pathways, eventually penetrating the brain parenchyma (Illum, 2004; Thorne and Frey, 2001). Nasal drug delivery has many advantages from a clinical perspective for its noninvasiveness, accessibility, and ease of administration. Recent reports confirm the positive outcome of nose-to-brain delivery not only for drug molecules with various molecular weights (Hanson et al., 2009; Yang et al., 2009), but also for living cells (Danielyan et al., 2009, 2011).

In this work we have investigated the possibility of using intranasal (iN) administration of aTf to protect and repair the neonatal white matter after a cerebral HI

Grant sponsors: The National Agency for Promotion of Science and Technology (Argentina), National Council of Scientific and Technical Investigation (Argentina), University of Buenos Aires.

*Correspondence to: Dr. Juana M. Pasquini, Departamento de Química Biolgica. Facultad de Farmacia y Bioquímica—Universidad de Buenos Aires, Junin 956 Buenos Aires 1113 Argentina. E-mail: jpasquin@qb.ffyb.uba.ar

Received 22 November 2011; Accepted 31 May 2012

DOI 10.1002/glia.22374

Published online in Wiley Online Library (wileyonlinelibrary.com).

event. Transgenic mice expressing the enhanced green fluorescent protein under the 2′-3′-cyclic nucleotide 3′-phosphodiesterase (CNP-EGFP) promoters were used. These animals provide a convenient fluorescent tag for OPCs and oligodendrocytes (OLs) in tissue slices (Yuan et al., 2002). Immediately after the HI insult a group of 10-day-old mice were iN treated with aTf. Human aTf was detected in all brain areas as soon as half an hour after a single iN administration. Western blot analysis showed high human aTf concentrations in different brain regions including the olfactory bulb, forebrain, and posterior brain of HI mice. Furthermore, our data suggest that the iN administration of aTf prevented white matter damage and OL loss, thus preventing OPC death by apoptosis and promoting their maturation. In conclusion, this work is relevant to developing means to induce neuroprotection and for myelin repair following cerebral HI in the neonatal brain.

MATERIAL AND METHODS

Intranasal Administration of aTf

Normal 10-day-old (P10) CNP-EGFP mice were placed on their backs and anesthetized with ketamine (150 mg kg^{-1}) and xylazine (15 mg kg^{-1}), and 4 μL of aTf (10 mg mL^{-1}) was given into the right naris using a fine tip. After 30 min a second dose of aTf was infused following the same procedure. In another set of experiments, P10 mice received an iN administration of 2 μL of cytochalasine B (0.5 mM), colchicine (0.5 mM) or vehicle (PBS) and 15 min later aTf was infused as described before. Brains were removed 30 min after the second dose of aTf and separated into six parts: right and left olfactory bulb, right and left forebrain, and right and left posterior brain. The forebrain and posterior brain were separated coronally at about bregma level. Brain tissue was stored at −80°C until further use. Brain concentration of human aTf was measured using an anti-human Tf antibody. To verify the penetration of aTf into the HI mouse brain, the same experiment was conducted in P10 mice immediately after the HI insult.

Perinatal HI

Cerebral HI was induced in P10 CNP-EGFP mice of either sex by a permanent unilateral common carotid artery ligation followed by systemic hypoxia as described by Ferriero et al., 1996, who adapted the method of Rice et al. (1981) for mice. Mice were anesthetized with ketamine (150 mg kg^{-1}) and xylazine (15 mg kg^{-1}). Once they were fully anesthetized, a midline neck incision was made; the right common carotid artery was isolated by blunt dissection and then ligated using 5-0 surgical silk. After 4 h of recovery, the animals were exposed to 60 min of humidified 8% O_2 and 92% N_2 at 37°C in a water bath. Control animals were separated from the dam for the same period of time. Immediately after HI, a group of animals received iN administration of aTf and another group received iN administration of saline solution as described above.

In this study, 47 out of 55 mice survived the HI event. Five of these mice were sacrificed due to severe weight loss 4 days after surgery. Four mice were not used for data analysis due to extended ipsilateral hemispheric atrophy. The remaining 38 mice were analyzed at different ages and 17 mice were used as controls. All experimental procedures were approved by the University of Buenos Aires Committee of Laboratory Animals and animal experimentation was in accordance with the National Institute of Health-Guide for the Care and Use of Laboratory Animals.

Western Blot Analysis

The olfactory bulb, forebrain, and posterior brain from different experimental conditions were homogenized using TOTEX lysis buffer. A 100 μg of protein sample from each structure were boiled for 5 min in Laemmli buffer containing 4% 2-mercaptoethanol. Proteins were separated by SDS/PAGE using 10% acrylamide-bisacrylamide gels and transferred onto polyvinylidene fluoride membranes. These were blocked for 2 h in PBS-T (PBS/0.1% Tween 20) containing 5% FCS, followed by incubation with anti-aTf (1/1,000, ICN Biomedicals) overnight at 4°C. Membranes were washed in PBS-T, incubated for 1 h in horseradishperoxidase-conjugated secondary antibodies (1/2,000) in blocking buffer, washed in PBS-T and then developed using 3-3′ diaminobenzidine/Niquel/H_2O_2 mixture. To confirm equal protein loading of all lanes, the same blots were reprobed with an anti-actin antibody. Densitometric analysis of the bands was performed using the Gel-Pro analyzer 4.0.

Brain Section Preparation

Animals were anesthetized with ketamine and xylazine and perfused through the left ventricle of the heart with 30 mL of PBS followed by a 4% solution of paraformaldehyde in PBS. The brains were carefully dissected out and postfixed in the same solution overnight, followed by thorough washing in PBS and cryoprotection in PBS/30% sucrose for 24 h. The tissue was then frozen and used for obtaining 30 μm cryostat coronal sections using a Leica CM1850 cryotome. The floating sections obtained from different areas of the brain were kept in PBS/glycerol (1:1) solution and stored at −20°C until use.

Immunohistochemistry

Floating brain sections were rinsed twice with PBS (pH 7.4), then again with PBS/0.1% Triton X-100 (only for cytosolic antigens) and blocked overnight with PBS containing 5% FCS. For indirect immunofluorescence, sections were incubated at 4°C with the following antibodies: anti-NG2 and anti-PDGFRα (1/200, Neuromics),

anti-Nestin (1/100, Neuromics), anti-GFAP-Cy3 (1/800, Sigma), and anti-cleaved-caspase-3 (1/200, Cell Signaling). Identification of mature OLs was carried out using anti-MBP (1/400, a generous gift of Dr A.T. Campagnoni, University of California at Los Angeles) and anti-CC-1 (1/200, Abcam). For BrdU immunostaining, sections were pretreated in 2 M HCl for 60 min at 37°C followed by extensive rinses in 0.1 M borate buffer, pH 8.5, and with PBS/0.1% Triton X-100. Afterward, tissue sections were blocked and incubated with a mouse monoclonal anti-BrdU (1/100, Roche). After treatment with primary antibodies, sections were rinsed with PBS and incubated for 2 h with the appropriate secondary antibody and 5 μM Höechst dye at room temperature. Sections were rinsed again with PBS, carefully placed on glass slides, dried overnight, and mounted with a fluorescence mounting medium.

Incorporation of Bromo-Deoxyuridine (BrdU)

Cell proliferation was examined using 5-bromo-2-deoxyuridine (BrdU, Sigma). For BrdU labeling, mice were operated at P10 and then given six consecutive intraperitoneal injections of BrdU (50 mg kg^{-1}) from P14 to P19. Animals were transcardially perfused on P24 and brain sections were prepared as described above.

Image Analysis and Quantification

Microscopic evaluation was performed by epifluorescence using an Olympus BX50 microscope or confocal microscopy for colocalization studies. Photographs were taken with a CoolSnap digital camera. Confocal images were performed by capturing a series, or stack, of images focused at regularly placed intervals through the *Z* axis of an area of interest. Subsequently, using the Image J software, a 3D reconstruction and surface plot graphics were done. Image J software was used for image analysis. CNP-EGFP positive cells and CNP-EGFP/caspase3 double positive cells per mm^2 were quantified by integrating data obtained from 100 μm^2 fragments throughout the external capsule of the *corpus callosum* (CC), striatum, and cortex in three consecutive sections of the bregma and middle dorsal hippocampus level. Quantification of CNP-EGFP/BrdU double positive cells was done in the same way in the external capsule of the CC and the results were also expressed as the number of positive cells per mm^2. In contrast, integrated optical density (IOD) of MBP positive staining was evaluated in the external capsule of the CC and the cerebral cortex in three consecutive sections of the bregma and middle dorsal hippocampus level, subtracting background staining. Control data were set at an arbitrary value of 100% immunoreactivity and results were expressed as a percentage of their own control. GFAP positive cells were counted in the striatum in 10–12 randomly chosen high power views (100 × 100 μm each) in three consecutive sections at bregma level and results were expressed as the number of positive cells per mm^2. For quantification of nestin IOD in the subventricular zone (SVZ), three consecutive sections at bregma level were used; the area including positive immunoreactive cells was manually selected with the appropriate software tool and IOD was determined and expressed as a percentage relative to the control condition. PDGFRα positive cells were counted in the periventricular area of the ipsilateral hemispheres in three consecutive sections at bregma level. Cell counting results were converted into cells per mm^2 using Abercrombie's correction (Abercrombie, 1946) and the mean value was used for representing one single brain. To evaluate neuronal damage, coronal sections at bregma level were used. The area of NeuN staining at the striatum was outlined manually using image processing tools (NIH Image J software) and the ratio of the ipsilateral to contralateral NeuN area was calculated (R = IL/CL). Evaluation of neocortical axonal demyelination was done by CNP-EGFP and β-III tubulin staining under different experimental conditions. Demyelinated axons were quantified at high magnification confocal photomicrographs randomly selected from the neocortex of the ipsilateral hemisphere.

Primary Cultures of Cortical Oligodendrocytes

Enriched OLs were prepared as described by Amur-Umarjee et al. (1993). First, cerebral hemispheres from 1-day-old mice were mechanically dissociated and were plated on poly-D-lysine-coated flasks in Dulbecco's modified Eagle's medium and Ham's F12 (1:1vol/vol) (Invitrogen), containing 100 μg mL^{-1} gentamycin and supplemented with 4 mg mL^{-1} dextrose anhydrous, 3.75 mg mL^{-1} HEPES buffer, 2.4 mg mL^{-1} sodium bicarbonate, and 10% fetal bovine serum (FBS) (Omega Scientific). After 24 h the medium was changed and the cells were grown in DMEM/F-12 supplemented with insulin (5 μg mL^{-1}), human transferrin (50 μg mL^{-1}), sodium selenite (30 nM), d-Biotin (10 mM), 0.1% BSA (Sigma), 1% horse serum, and 1% FBS (Omega Scientific). After 9 days, OPCs were purified from the mixed glial culture by the differential shaking and adhesion procedure of Suzumura et al. (1984) and allowed to grow on polylysine-coated coverslips in defined culture media (Agresti et al., 1996) plus PDGF-AA (10 ng mL^{-1}) and bFGF (10 ng mL^{-1}) (Peprotech). The following day (*in vitro* day 2) the media was changed and cells were treated with fresh media, in the presence or absence of human transferrin (100 μg mL^{-1}). Hypoxia was maintained for 12 h by incubating the cells in a Napco 7001 incubator (Precision Scientific, Chicago), which contained a humidifying water pan infused with 5% CO_2 and 95% N_2 to achieve the desired concentration of hypoxia.

Caspase-3 Assay

NucView488 Caspase-3 substrate, a novel cell-membrane-permeable fluorogenic caspase substrate designed

for detecting caspase-3 activity within live cells in real time, was used in accordance with the manufacturer's recommendations (Biotium). One day after plating (*in vitro* day 2), OPC primary cultures were incubated in defined culture media (Agresti et al., 1996) containing NucView488 Caspase-3 substrate (final concentration 5 μM) in a stage top chamber at 37°C, which was placed on the stage of a spinning disc confocal inverted microscope (Olympus, IX81-DSU) equipped with a CCD camera (Hamamatsu ORCA-ER). Hypoxia was maintained during the entire time-lapse experiment (6 h) by incubating the cells in the microscope stage chamber, which contained a humidifying water pan infused with 5% CO_2, 1% O_2, and 94% N_2. Fluorescent field images were obtained with a specific GFP filter at 6-min intervals for a total of 6 h. SlideBook 4.1 software was used to assess apoptotic cell death by calculating the percentage of Caspase-3 positive cells in a total of five experiments on four random fields. Parallel experiments were performed using immature OLs. Immature OLs were obtained from OPC primary cultures by growing the cells in a mitogen-free medium (mN2) (Oh et al., 2003) for 4 days. mN2: DMEM/F-12 supplemented with D-glucose (4.5 g L^{-1}), insulin (5 μg mL^{-1}), human transferrin (50 μg mL^{-1}), sodium selenite (30 nM), T3 (15 nM), d-Biotin (10 mM), hydrocortisone (10 nM), 0.1% BSA, 1% horse serum, and 1% FBS.

Immunocytochemistry

Cells were stained with antibodies for several OL markers and examined by confocal microscopy. For Sox2, Sox9, Olig2, CC1, and MBP immunostaining, the cells were rinsed briefly in PBS and fixed in 4% buffered paraformaldehyde for 30 min at room temperature. After rinsing in PBS, the cells were permeabilized with 0.1% Triton X-100 in PBS for 10 min at room temperature and then processed for immunocytochemistry following the protocol as outlined by Reyes et al. (2002). Essentially, fixed cells were incubated in a blocking solution (5% goat serum in PBS) followed by an overnight incubation at 4°C with a primary antibody for Sox2 (1:200), Sox9 (1:500), Olig2 (1:500), CC1 (1:300), and MBP (1:800). Staining with NG2 (1:100) was performed on live cells without permeabilization for 1 h at room temperature before fixation. The primary antibodies were all purchased from Chemicon/Millipore. Cells were then incubated with the appropriate secondary antibodies (1:200; Jackson) and mounted onto slides with Aquamount (Lerner Laboratories); fluorescent images were obtained using an Olympus spinning disc confocal microscope. Nuclei were stained with the fluorescent dye Hoechst 33342 (5 μg mL^{-1} in 1% DMSO) to determine the total number of cells. Quantitative analysis of the results was done counting the antigen-positive and Hoechst-positive cells in 20 randomly selected fields, which resulted in counts of >2,000 cells for each experimental condition. Counts of antigen-positive cells were normalized to the counts of total Hoechst-positive cells for each condition.

Statistics

Statistical analysis was performed using GraphPad Prism 4.03 software by analysis of variance followed by Newman–Keuls multiple comparison test. A $P < 0.05$ was considered statistically significant. Data are given as the means ± S.E.M.

RESULTS

Human aTf Diffused into the Neonatal Brain After Intranasal Administration

To determine whether iN administration of human aTf reaches the different brain areas and provides neuroprotection to the neonatal brain following cerebral HI, aTf was infused into the right naris of postnatal-day-10 (P10) mice. Two infusions of aTf (10 mg mL^{-1}) were given into the right naris separated by 30 min. Thirty minutes after the second dose, brains were removed and separated into six parts: right and left olfactory bulb (OB), right and left forebrain (FB), and right and left posterior brain (PB). Experiments were done with or without a prior HI insult performed by right common carotid artery ligation followed by exposure to low oxygen concentration (8%) for 1 h. As shown in Fig. 1A, a high concentration of aTf was seen in the right OB 30 min after the second aTf dose in control brains (0.063 ± 0.015 μg/100 μg). Human aTf concentration in the right FB and PB was 0.018 ± 0.002 and 0.028 ± 0.004 μg/100 μg protein, respectively, which was about 30 and 40% of that in the right OB. In the HI group, aTf concentration in the right OB was similar to that in the control group 1 h post iN administration (0.091 ± 0.029 μg/100 μg). However, 30 min after the second aTf dose the concentration in the right FB and PB was 0.042 ± 0.007 and 0.063 ± 0.012 μg/100 μg, respectively, which was significantly higher than that in the control brains (Fig. 1A). Additionally, human aTf was also found in the contralateral hemispheres of HI-treated mice (data not shown). Furthermore, 24 h after the iN administration, aTf was not detected in either the HI-treated or untreated control brains (data not shown). It is important to point out that we found a significant decrease in aTf concentrations in the OB when different cytoskeleton venoms, such as cytochalasin B and colchicine, were iN-administered before aTf (Fig. 1B), which suggests that active axonal transport is essential for aTf delivery into the brain.

Intranasal Administration of aTf Reduced Brain Injury After an HI Incident

Two days after the HI incident (P12), brain coronal sections were analyzed from all the experimental groups. Measurements were done in different areas of the CNS such as cortex, corpus callosum (CC), external capsule and striatum (Fig. 2). A loss of CNP-EGFP positive cells was clearly observed in the ipsilateral

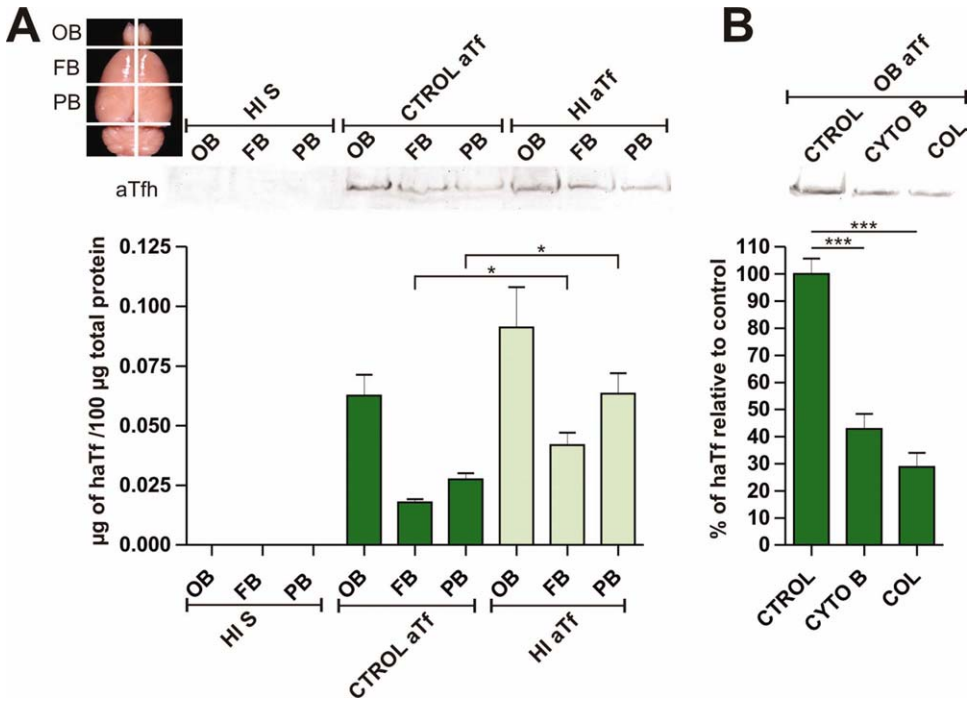

Fig. 1. Western blot analysis of aTf in different brain areas. (**A**) Protein lysates of olfactory bulb (OB), frontal (FB), and posterior brain (PB) were obtained from the right hemisphere of control (Control) and HI mice treated iN with aTf or saline solution (S). Assays were done 30 min after the second dose of aTf and aTf concentration in each area was calculated using aTf standards. Concentrations were calculated as µg of aTf present in each structure per 100 µg of total protein. (n = 3 HI S; n = 3 HI aTf, and n = 3 Control) (**B**) Western blot analysis of aTf in protein lysates of OB from mice that received either saline (Control) or the cytoskeleton venoms, cytochalasin B (CYTO B) or colchicine (COL) 15 min before the iN administration of aTf (n = 3 Control; n = 3 CYTO B, and n = 3 COL). Values are the means ± S.E.M of three independent experiments. *$p < 0.05$, ***$P < 0.001$ vs. respective controls. [Color figure can be viewed in the online issue, which is available at wileyonlinelibrary.com.]

hemisphere of the untreated HI animals (Fig. 2A). Interestingly, the decrease in the number of these cells was significantly lower in HI animals treated with human aTf (Fig. 2A). Immunohistochemical analysis for MBP exhibited a similar outcome, with the aTf-treated mice showing a reduced loss of MBP immunolabeling after the HI injury, while the untreated mice showed a more drastic reduction in MBP immunolabeling after the HI insult (Fig. 2B). Figure 3 shows high magnification images of the external capsule of the CC, cerebral cortex, and striatum. The number of CNP-EGFP was significantly lower in the HI CC compared with control or aTf-treated tissue 2 days post injury. CNP-EGFP positive cells showed high complexity in controls and aTf-treated animals, but were either bipolar or apoptotic in those treated with saline solution (Fig. 3B).

Two weeks after the cerebral HI (P24), coronal sections of the CC and cortex showed significantly diminished immunostaining for MBP in untreated HI mice (Fig. 4A,B). In contrast, aTf-treated animals displayed normal MBP levels in both the CC and cortex, suggesting complete remyelination at P24 (Fig. 4A,B). When CNP-EGFP positive cells were quantitated in the CC, the same phenomena was observed: untreated HI mice exhibited 375 ± 34 cells mm^{-2}, while those treated with aTf showed 454 ± 20 cells mm^{-2} CNP-EGFP positive cells (Fig. 4C). In addition, we found that the majority of these CNP-EGFP-expressing cells colocalized with CC-1 in all the experimental conditions (Fig. 4C).

HI encephalopathy in term newborns produces chronic neurological disability in survivors due to neuronal loss. Although experimental HI injury in the immature rodent brain is well established in the literature, the extent of neuron injury varies with species and strains. In our model, we found a significant reduction in the number of striatal neurons 5 days after the HI damage (57% ± 26% NeuN area loss) and this reduction was significantly lower in the HI mice treated with aTf (15% ± 14% NeuN area loss) (Fig. 5A). We were unable to detect neocortex neurodegeneration using βIII tubulin and NeuN staining; however, demyelinated axons of neurons that connect the neocortex with the CC were clearly seen in the HI mice (8 ± 3 demyelinated axons/200 μm^2). As expected, aTf treatment protected these axons against demyelination (3 ± 3 demyelinated axons/200 μm^2) (Fig. 5B).

It is becoming evident that neuroinflammation plays an important role in the loss of OLs and neurons after an HI insult in the preterm brain (Cai et al., 2006; Carty et al., 2008; Fan et al., 2006). In our model we noticed a substantial increase in GFAP-positive astrocytes 2 days after the HI event (Fig. 6). At P12, we found an approximate fivefold increase in the number of GFAP positive cells in the striatum of untreated and

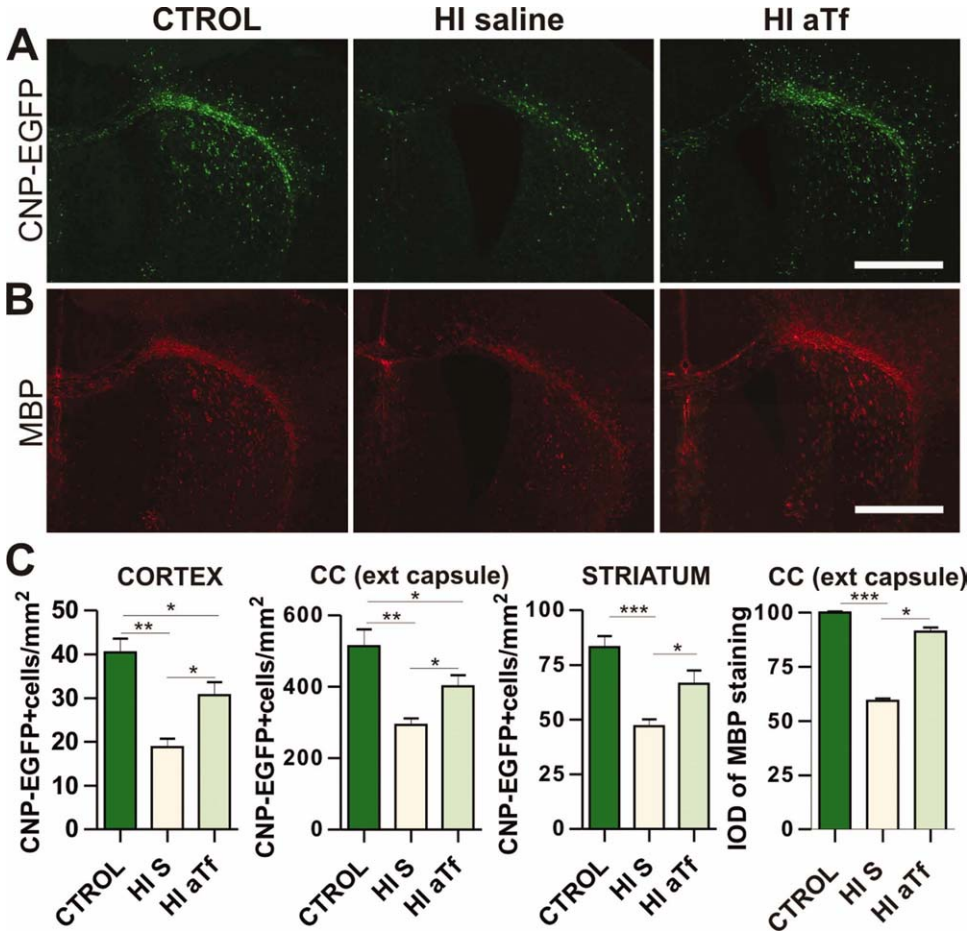

Fig. 2. CNP-EGFP and MBP expression in the brain of HI animals. (**A**) Evaluation of CNP-EGFP positive cells at P12. (**B**) Coronal sections of the brain were immunostained with anti-MBP at P12 in the different experimental groups. Scale bar = 1 mm. (**C**) Quantification of CNP-EGFP positive cells in three different brain areas and evaluation of MBP immunoreactivity by IOD in the external capsule of the CC. Values are expressed as the means ± S.E.M of three independent experiments (n = 6 HI S; n = 7 HI aTf; and n = 5 Control; $^{*}P < 0.05$, $^{**}P < 0.01$, and $^{***}P < 0.001$ vs. respective controls). [Color figure can be viewed in the online issue, which is available at wileyonlinelibrary.com.]

aTf- treated HI animals, with no significant differences among the two groups (Fig. 6A,C). However, 5 days after the HI injury (P15) animals treated with aTf showed a lower number of reactive astrocytes compared with untreated HI animals (443 ± 148 cells mm^{-2} vs. 644 ± 258 cells mm^{-2}, respectively) (Fig. 6A,C). In agreement with these data, double immunostaining for GFAP and S100β at P15 clearly revealed higher numbers of reactive astrocytes in the untreated HI group, probably due to more extended brain damage and demyelination (Fig. 6B,C). Finally, 2 weeks after the HI event (P24), the number of GFAP-expressing cells decreased in both experimental groups, although in both cases it was still twice as high as in control animals (Fig. 6A,C).

Effect of Intranasal Administration of aTf in the Subventricular Zone

Two days after cerebral HI we found a significant increase in the number of nestin-positive cells in the SVZ of brains treated with aTf (Fig. 7A). There was a 1.8-fold increase compared with controls, and a 1.6-fold increase compared with untreated HI animals (Fig. 7A). Similarly, we found an increase in nestin positive cells in both mouse groups compared with control animals at P15 (Fig. 7A). Although not statistically significant, there was a tendency for a higher increase in untreated mice than in those treated with aTf (Fig. 7A), which suggests that, in the latter condition, the number of cells expressing nestin in the SVZ had already started to decrease. Furthermore, our results showed that the nestin positive progenitors found in the HI aTf condition expressed low levels of GFAP at P12 (30% ± 6%). In contrast, nestin-positive cells peaked later (P15) in the HI untreated mice and expressed high levels of GFAP (66% ± 9%) (Fig. 7A). In Fig. 7B high magnification images of the lateral wall of the SVZ show PDGFRα/CNP-EGFP double positive OPCs (arrows) in the HI mice. Two days after the HI event (P12) the number of PDGFRα-positive OPCs was higher in mice treated with aTf than in untreated brains (149 ± 105 vs. 367 ± 40 cells mm^{-2}) (Fig. 7B).

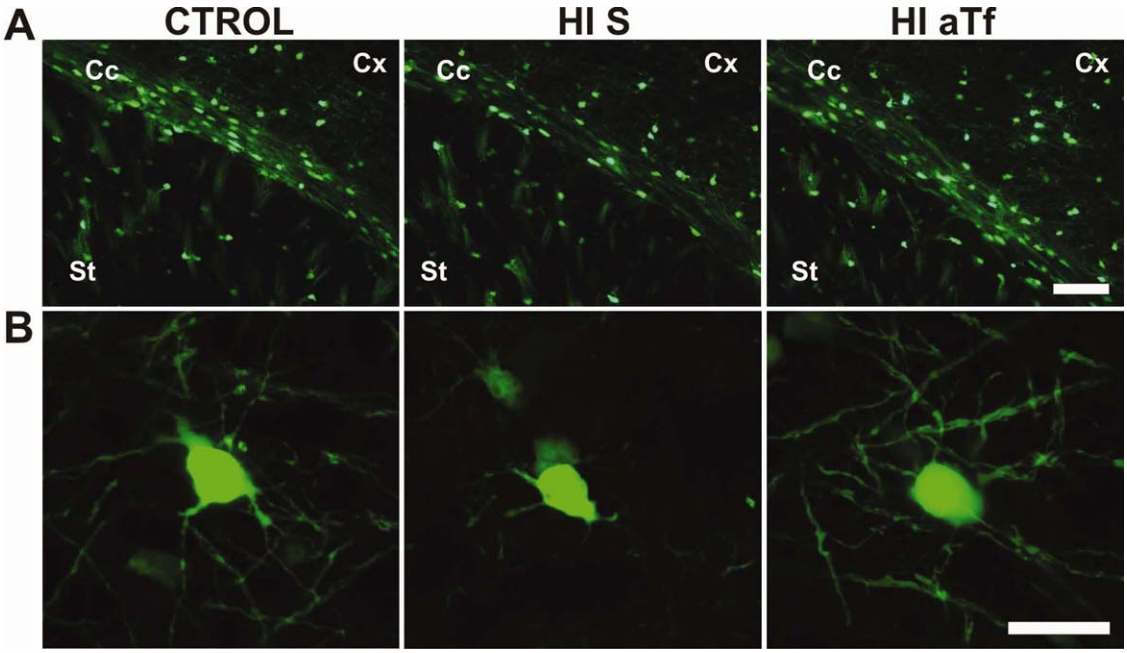

Fig. 3. Myelin loss post HI injury. (**A**) CNP-EGFP positive cells in the external capsule of the CC in the control, untreated and aTf-treated HI mice at P12. Scale bar = 100 μm. (**B**) Higher magnification confocal photomicrographs of representative CNP-EGFP positive cells in the different experimental conditions are shown. Scale bar = 10 μm. CC: external capsule of corpus callosum; Cx: cerebral cortex; and St: striatum. [Color figure can be viewed in the online issue, which is available at wileyonlinelibrary.com.]

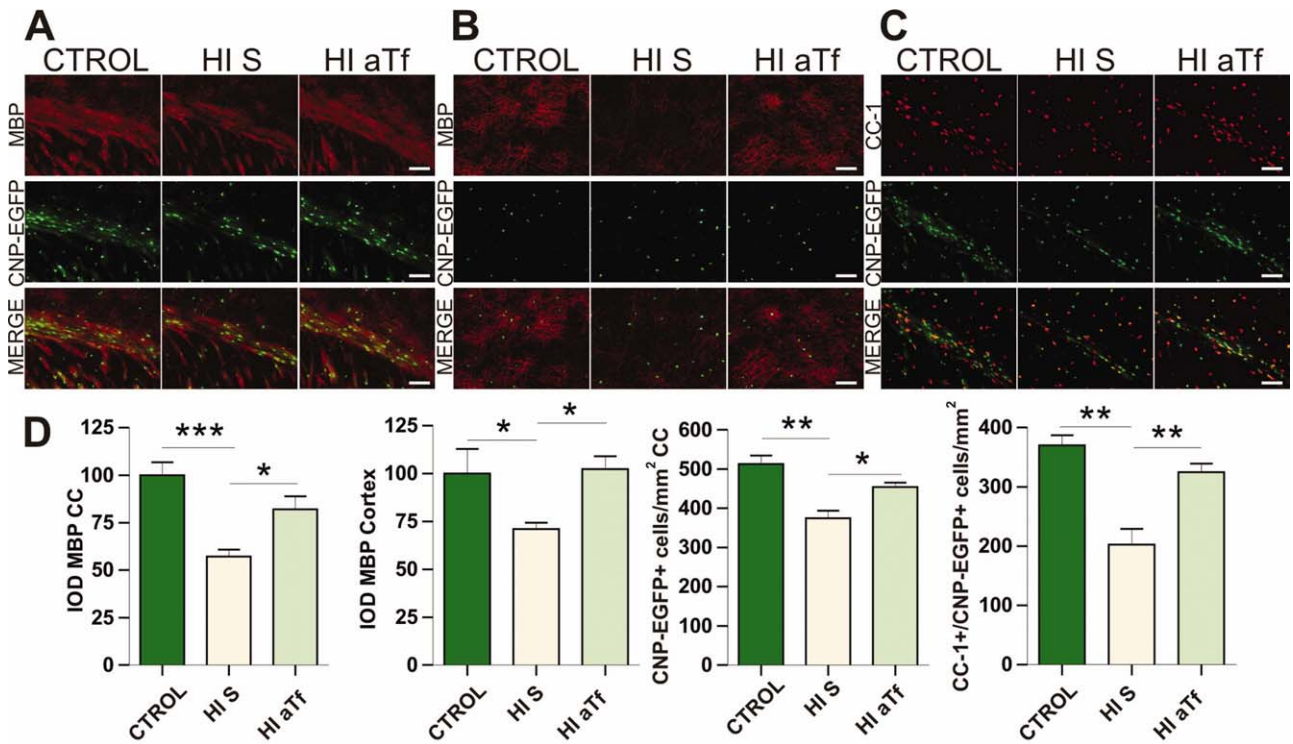

Fig. 4. Remyelination after HI damage. (**A**) MBP immunoreactivity and CNP-EGFP positive cells were analyzed in the external capsule of the CC under different experimental conditions at P24. Colocalization of both markers is also shown. (**B**) MBP/CNP-EGFP colocalization was also evaluated in the cerebral cortex at the same time point. (**C**) CC-1 immunoreactivity in the external capsule of the CC and its colocalization with CNP-EGFP is shown. (**D**) Values are expressed as the means ± S.E.M of three independent experiments (n = 6 HI S; n = 6 HI aTf; and n = 6 Control; $^{*}P < 0.05$, $^{**}P < 0.01$, and $^{***}P < 0.001$ vs. respective controls). Scale bar = 100 μm. [Color figure can be viewed in the online issue, which is available at wileyonlinelibrary.com.]

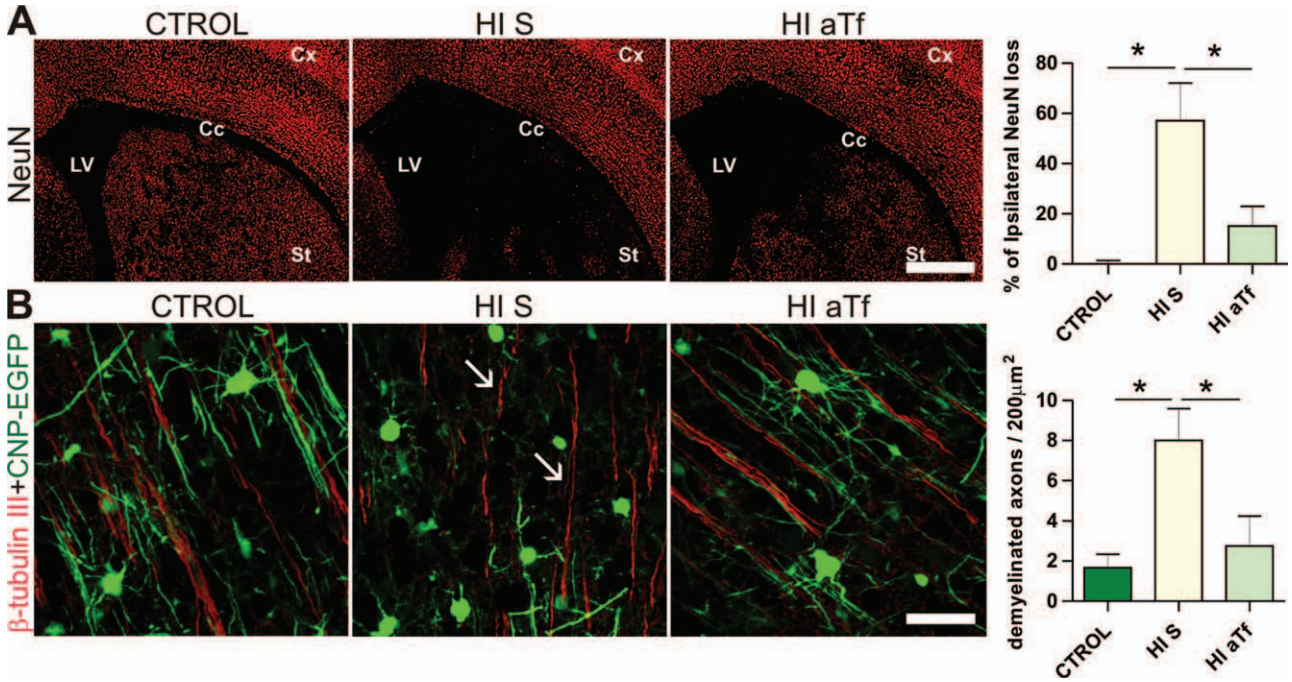

Fig. 5. Neuronal loss after the HI event. (**A**) Brain sections of the different experimental conditions were immunostained for NeuN at P15. Scale bar = 600 µm. The percentage of NeuN area loss in comparison with the contralateral hemisphere for each experimental condition was quantified. The results are expressed as the means ± S.E.M of three independent experiments. (**B**) High magnification confocal images from the neocortex showing CNP-EGFP positive OLs and axonal fibers identified by the anti-β-tubulin III antibody. Scale bar = 40 µm. The number of demyelinated axons (arrows) in each experimental condition was quantified. Values are expressed as the means ± S.E.M of three independent experiments (n = 6 HI S; n = 7 HI aTf; and n = 6 Control; *$P < 0.05$ vs. respective controls). Cc: corpus callosum; Cx: cortex; St: striatum; Lv: lateral ventricle.

Intranasal Administration of aTf Promoted OPC Proliferation and Inhibited Apoptotic Cell Death After HI

OPC proliferation was estimated using immunodetection of BrdU incorporation. Proliferating OPCs were identified by immunofluorescence for BrdU and CNP-EGFP, and the relative number of CNP-EGFP/BrdU-positive cells was quantified in each experimental group (Fig. 8). After the HI happening, BrdU was injected daily from P14 to P19 and animals were sacrificed 2 weeks after the HI injury (P24). Our results show that cerebral HI induced proliferation of OPCs (Fig. 8). In the CC the number of CNP-EGFP/BrdU double positive cells was significantly higher in the ipsilateral brain after cerebral HI as compared with the sham brain (1.8-fold increase). As expected, post-treatment with aTf further increased (1.5-fold) the number of CNP-EGFP/BrdU double positive cells as compared with the vehicle-treated control group (Fig. 8).

Apoptotic cell death was measured using a specific antibody which detects caspase-3 activity within individual cells. The number of caspase-3/CNP-EGFP double positive cells was quantified in the ipsilateral cortex, striatum, and CC of HI mice at P12 (Fig. 9A). We found a fourfold increase in the number of caspase-3 positive-cells in the CC and striatum and a fivefold increase in the cortex of untreated HI mice (Fig. 9A). In contrast, the number of apoptotic cells returned to near control levels in the CC and striatum and decreased significantly in the cortex when HI animals were treated with aTf (1.8-fold decrease as compared with control mice) (Fig. 9A).

aTf-Treated OPCs are More Resistant to Death by Apoptosis Under Low Oxygen Concentrations

We also evaluated OL apoptotic cell death *in vitro*. For these studies we used a real-time caspase-3 assay which detects caspase-3 activity within individual living cells. This assay is bi-functional in the sense that it can both detect intracellular caspase-3 activity and stain the cell nucleus, which undergoes morphological changes during the apoptotic process. Cultured OPCs were incubated in a stage top chamber with 5% CO_2 and 1% O_2 at 37°C, which was placed on the stage of a spinning disc confocal inverted microscope. Using this system we followed the response of cultured OPCs to a low oxygen atmosphere (1%) in real-time, as well as the role of aTf in protecting OPCs during this *in vitro* hypoxic insult. Examples of such measurements are shown in Fig. 9B. Consistent with the preceding results, the combined use of real time confocal microscopy and the caspase-3 indicator revealed that OPCs displayed a significant increase in the percentage of caspase-3-positive cells after 6 h of culture in a low oxygen atmosphere (Fig. 9B). Parallel experiments performed with hypoxic OPCs

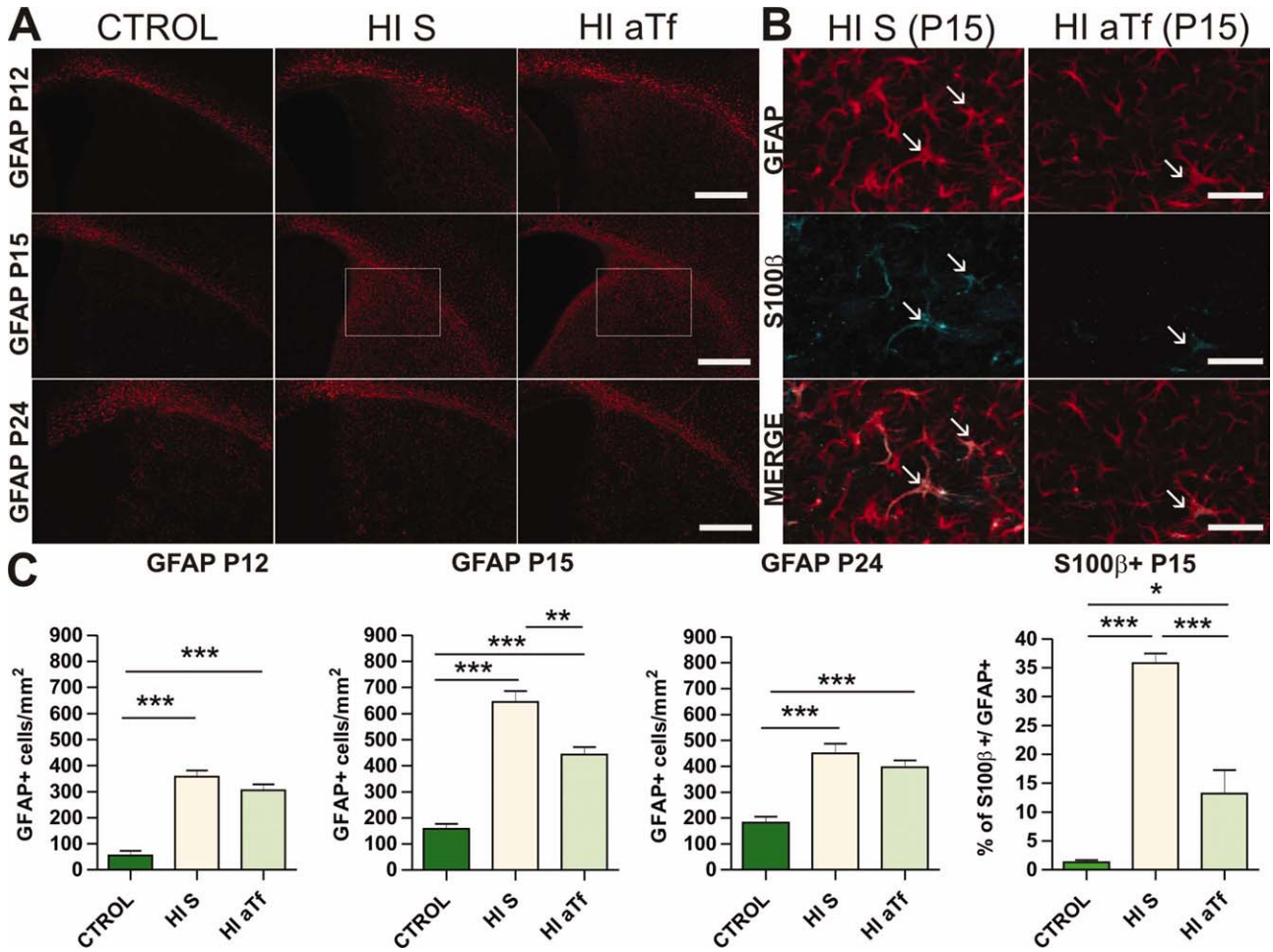

Fig. 6. Astrocyte activation in the striatum of HI mice. Coronal sections of the brain were immunostained with anti-GFAP at different time points after cerebral HI in the different experimental groups. Values are expressed as the means ± S.E.M of three independent experiments. At least three animals per condition were analyzed; $^{*}P < 0.05$, $^{**}P < 0.01$, and $^{***}P < 0.001$ vs. respective controls. Scale bar = 100 μm. [Color figure can be viewed in the online issue, which is available at wileyonlinelibrary.com.]

grown in the presence/absence of aTf clearly showed a significant reduction in caspase labeling when aTf was added to the culture medium (Fig. 9B). Additionally, and to establish the impact of low oxygen exposure at distinct stages of OL maturation, OPCs were treated with aTf and subjected to hypoxic culture conditions after switching the cells to a mitogen-free medium (mN2). Under these conditions there was a general decline in early immunocytochemical markers, such as NG2, and an increase in intermediate (e.g., 04) and mature (e.g., GC, MBP) markers consistent with OPC differentiation (Paez et al., 2009). Interestingly, in this more mature OL population subjected to hypoxic culture conditions, we found no significant differences among experimental groups (Fig. 9C). These *in vitro* data suggest that aTf is effective in protecting immature OLs during a hypoxic event and reveal that mature OL are more resistant to apoptotic death under hypoxic culture conditions. In addition, and under the same experimental conditions, we found a significant decrease in the number of OPCs expressing immature markers, such as Sox2 and NG2, and also an increase in cells expressing OL mature markers such as CC1 and MBP after 12 h of aTf treatment (Fig. 10A). This effect was much more evident under low oxygen concentration, which suggests that aTf further promotes OPC differentiation under hypoxic culture conditions (Fig. 10B). Moreover, since mature OL are more resistant to low oxygen concentration, these results indicate that aTf might be protecting OPCs against the hypoxic insult by promoting their differentiation.

DISCUSSION

Intranasal Infusion is an Effective Approach to Delivering aTf into the Brain

The blood–brain barrier presents a major problem in developing treatment for CNS diseases, as it prevents a number of potentially therapeutic agents from reaching

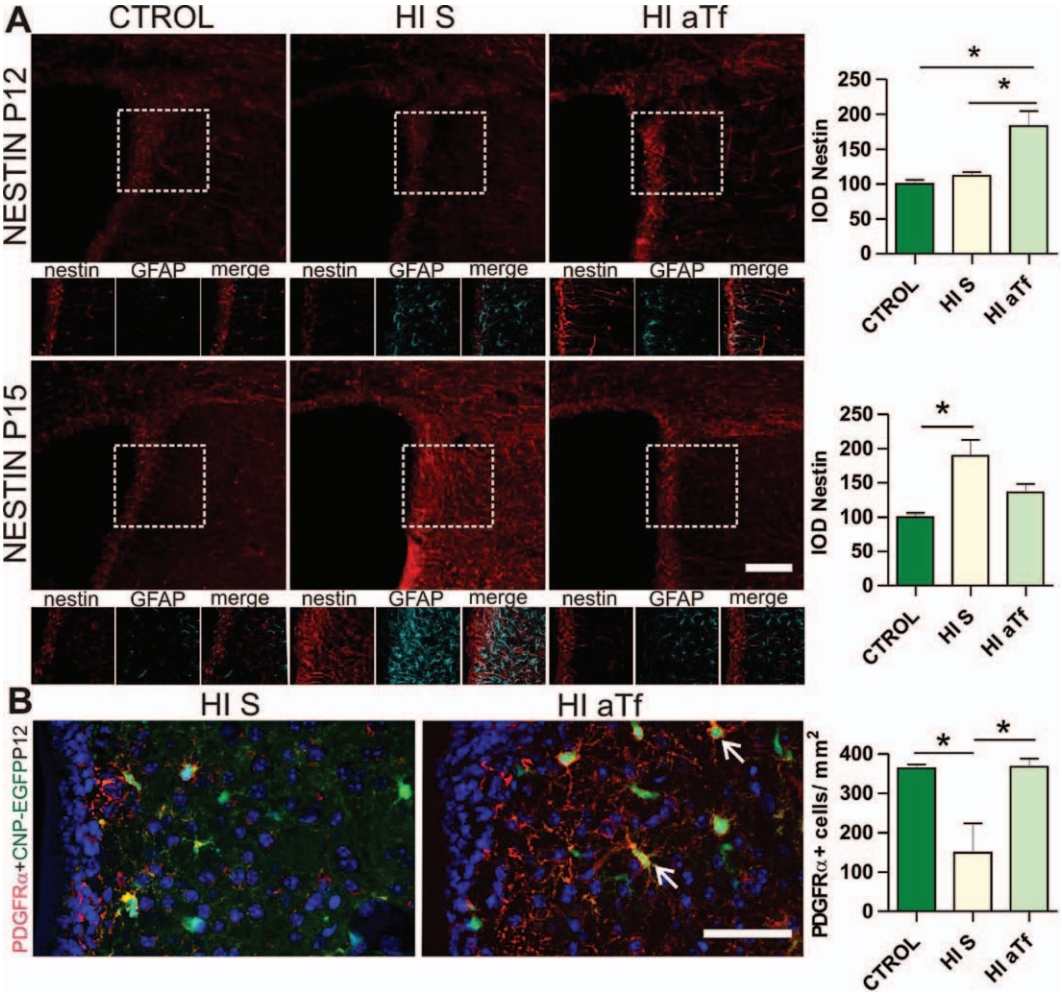

Fig. 7. Nestin and PDGFr expression in the SVZ. (**A**) Representative coronal sections of the dorsolateral SVZ immunostained with anti-nestin in the different experimental groups 2 days (P12) and 5 days (P15) after the HI incident. Scale bar = 100 μm. Insets show nestin/GFAP colocalization under the different experimental condition. (**B**) High magnification confocal images showing PDGFrα/CNP-EGFP double positive OPCs (arrows) in the lateral wall of the SVZ in untreated (HI S) and aTf-treated HI mice, 2 days (P12) after HI. Scale bar = 40 μm. Values are expressed as the means ± S.E.M of three independent experiments (n = 6 HI S; n = 7 HI aTf; n = 6 Control; $^{*}P < 0.05$, $^{**}P < 0.01$, $^{***}P < 0.001$ vs. respective controls).

the brain. Apotransferrin, a promising treatment for various brain injuries has been shown to provide neuroprotection to newborn rats (Adamo et al., 2006; Guardia Clausi et al., 2010). However, delivery to the brain remains problematic to the use of these agents. The iN administration of neurotrophic factors and other substances, including certain hormones, has received increasing attention in recent years. The olfactory region provides both extra and intracellular pathways into the CNS, bypassing the blood–brain barrier. A direct extracellular pathway between the nasal passages and the brain was first conclusively demonstrated for horseradish peroxidase (Balin et al., 1986). There are several reports on successful iN administration of insulin-like growth factor-1 (IGF-1) in the treatment of various brain injuries. Results by Thorne and Frey (2001) show that IGF-1 administered intranasally in rats can reach distant areas such as the cerebral cortex, the hypothalamus, the cerebellum, the brain stem, and the medulla in concentrations considered to be of therapeutic value. In addition, iN administration of IGF-1 has been found to reduce infarct volume and improve neurological function in adult rats following middle cerebral artery occlusion (Liu et al., 2001a,b). Moreover, three different neuropeptides have been intranasally delivered to human patients, showing that they bypass the bloodstream entering the CNS within 30 min (Born et al., 2002).

In the current study, we have shown that aTf was present in the right OB, FB, and PB in both the control and HI animals after iN administration. More important, aTf concentration was higher in HI animals than in control mice. Accordingly, it has been reported that a cerebral HI insult enhances the movement of exogenous compounds such as IGF-1 into the cerebrum through white matter tracts and perivascular spaces (Guan et al., 1996).

The mechanisms of protein transport from the nasal cavity to the brain are not entirely known, although several possible pathways have been proposed (Thorne

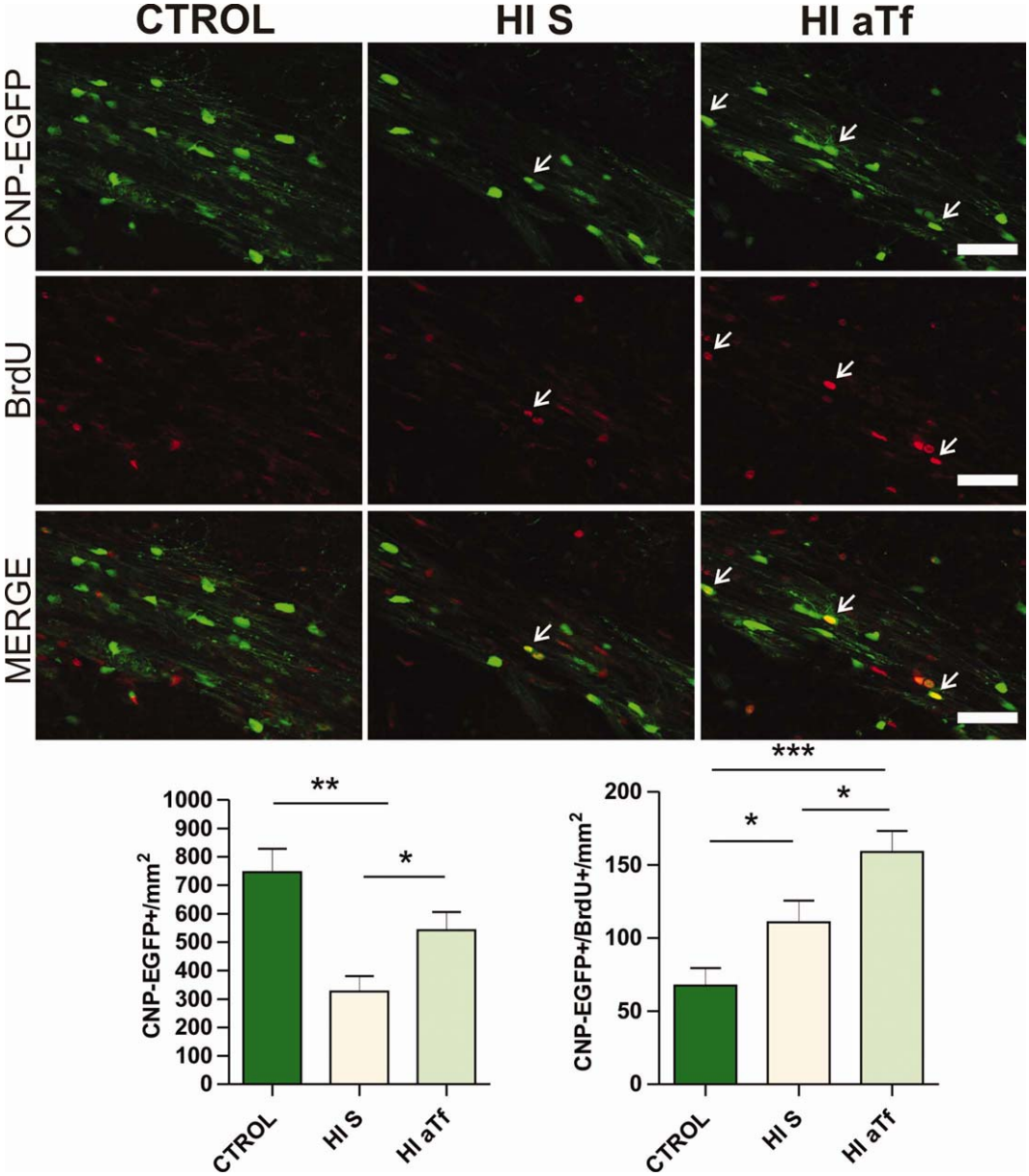

Fig. 8. OPC proliferation after HI. Four days after the HI injury (P14) animals received six consecutive BrdU injections from P14 to P19. Five days later (P24) brain coronal sections from control, HI S, and HI aTf mice were obtained for BrdU immunodetection. The number of CNP-EGFP and CNP-EGFP/BrdU double positive cells (arrows) were evaluated in the external capsule of the CC. Values are expressed as the means ± S.E.M of three independent experiments (n = 6 HI S; n = 6 HI aTf; and n = 6 Control; $^{*}P < 0.05$, $^{**}P < 0.01$; and $^{***}P < 0.001$ vs. respective controls). Scale bar = 100 μm. [Color figure can be viewed in the online issue, which is available at wileyonlinelibrary.com.]

et al., 1995). In agreement with previous results (Moos et al., 2011), our data indicate that anterograde axonal transport is essential for aTf delivery into the perinatal mouse brain. Supporting this conclusion, a very low concentration of aTf was detected in the OB when cytochalasine B or colchicine was administered before the iN administration of aTf. Colchicine inhibits microtubule assembly and reduces axonal transport (Han et al., 1998; Hastie, 1991) while an intravitreal injection of cytochalasin B has been shown to inhibit neurofilament axonal transport in optic axons (Jung et al., 2004).

Although our findings demonstrated the potential for using iN infusion as a novel noninvasive delivery method to target aTf to the brain, more fundamental studies are required. Future studies are necessary to determine the exact transportation route of aTf from the olfactory region to the brain, its subsequent clearance, and its possible side effects.

aTf Protects Neonatal White Matter After an HI Incident.

We have previously reported that a single intracranial injection of aTf upregulates the expression of diverse myelin constituents and significantly increases myelin

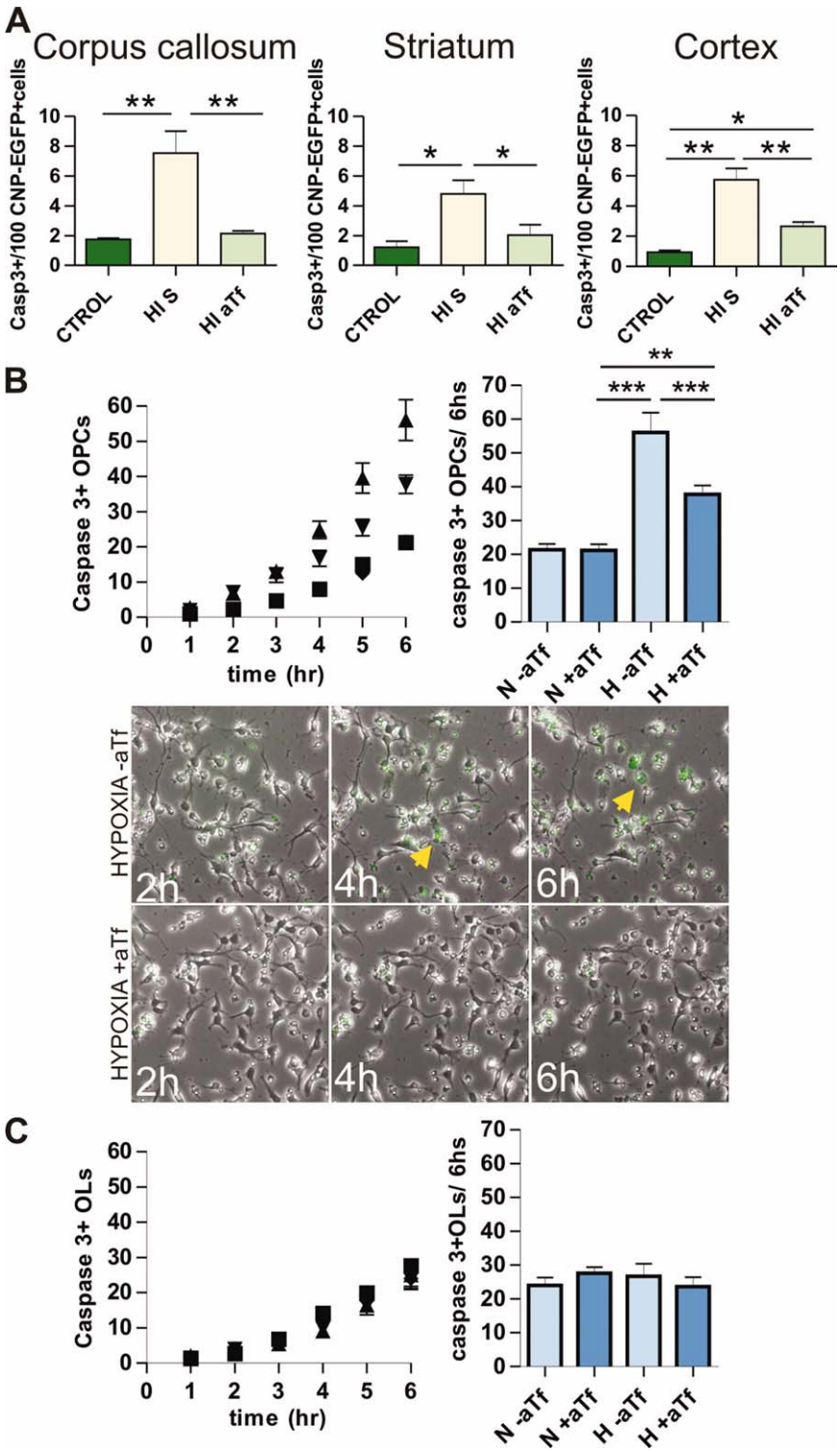

Fig. 9. aTf inhibits apoptotic cell death post HI in vivo and in vitro. (**A**) Double positive cells for caspase3 and CNP-EGFP in the ipsilateral CC, striatum, and cerebral cortex were counted 2 days after (P12) the HI insult. Values are expressed as the means ± S.E.M of three independent experiments (n = 6 HI S; n = 7 HI aTf; and n = 5 Control; $^{*}P < 0.05$, $^{**}P < 0.01$, and $^{***}P < 0.001$ vs. respective controls). (**B**) Caspase 3 activity in primary cultures of OPCs. Caspase 3 activity was detected in real-time using NucView™ 488 substrate as described in Materials and Methods. Fluorescent field images were obtained with a specific GFP filter at 6-min intervals for a period of 6 h. Brightfield images were superimposed to show cell morphology. Representative images of hypoxic OPCs in the presence or absence of aTf are shown. Yellow arrowheads designate some apoptotic OPCs (caspase 3-positive cells). (**C**) Parallel studies were done in immature OLs. Results in B and C were expressed as the number of caspase 3-positive cells per hour or as the total number of caspase 3-positive cells per 6 h. Results are the means ± SEM for three independent experiments. $^{*}P < 0.05$; $^{**}P < 0.01$ compared with controls. ■ (Normoxia+aTf); ▼ (Hypoxia aTf); ▲ (Hypoxia-aTf); ♦ (Normoxia-aTf). **N**: Normoxia; **H**: Hypoxia. [Color figure can be viewed in the online issue, which is available at wileyonlinelibrary.com.]

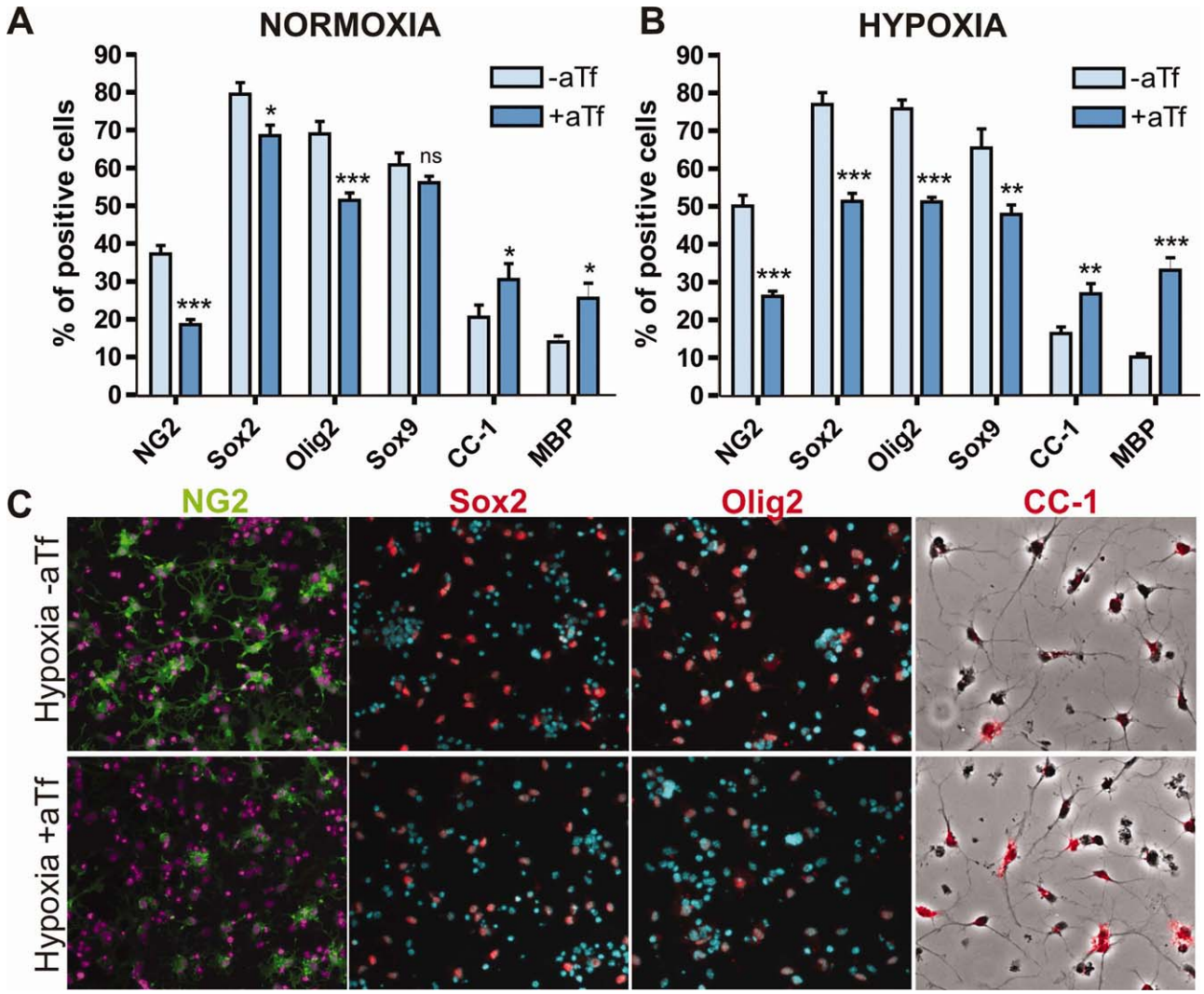

Fig. 10. aTf promotes OPC maturation under hypoxic culture conditions. (**A, B**) Enriched OPC cultures from 1-day-old mice were incubated for 12 h in defined culture medium with or without aTf (100 μg mL^{-1}) under normal or hypoxic conditions. After treatment, cells were fixed and immunostained for several OL markers and the percentage of positive cells in each experimental condition was analyzed by confocal microscopy. Results are the means ± SEM for three independent experiments.*$P < 0.05$, **$P < 0.01$, and ***$P < 0.001$ vs. respective controls. N: Normoxia; H: Hypoxia. (**C**) Representative photomicrographs showing NG2; Olig2; Sox2; and CC1 positive cells after 12 h of hypoxia in the presence or absence of aTf. [Color figure can be viewed in the online issue, which is available at wileyonlinelibrary.com.]

deposition, especially in areas close to the lateral ventricles in rats (Escobar Cabrera et al., 1994, 1997, 2000; Marta et al., 2003). This promyelinating effect was also seen in primary cultures of OLs (Paez et al., 2002), as well as in N19 and N20.1 cell lines treated with aTf (Paez et al., 2004). These data were confirmed by other authors who showed that aTf regulates MBP expression (Espinosa de los Monteros et al., 1999; Espinosa-Jeffrey et al., 2002) and that transgenic mice overexpressing the human Tf gene evidence increased myelination (Saleh et al., 2003).

We have recently demonstrated that aTf plays a functional role in a model of HI in the neonatal rat brain (Guardia Clausi et al., 2010). A number of papers have discussed this matter and a special mention can be made of that of Back et al. (2006), which supported the idea that hypoxia inhibits OL maturation, and that caffeine administration during postnatal development may be useful in the prevention of periventricular leukomalacia. In contrast, intraventricular administration of insulin-like growth factor-1 after HI rescues OPCs in the perinatal white matter when given after the insult (Wood et al., 2007). Results of Fan et al. (2006) show that minocycline has long-lasting protective effects in the neonatal rat brain in terms of HI-brain injury.

Similar to previous studies, in this article we have found that a HI event in the neonatal brain produced severe demyelination of the CC, cortex, external capsule, and striatum. Hypomyelination was accompanied by astrogliosis and apoptotic cell death. Astroglial activation began to increase 2 days, and peaked 5 days after the HI event in the striatum. Reactive astrocytes expressing high levels of S100β, a protein associated with neurotoxic effects (Yasuda et al, 2004), were also

found at different time points post-HI. Furthermore, we found a significant neuronal loss in the striatum of these mice 5 days after the HI injury. In contrast, aTf treatment reduced astrogliosis and neuronal loss in the striatum of HI animals and increased the survival of OLs in the CC, cortex, and striatum at different time points after the HI event. Histological examination in brain tissue of aTf-treated HI animals revealed a great number of mature OLs repopulating the CC and cortex, as compared with untreated controls. MBP staining gradually increased, reaching normal levels at P15. In contrast, reduced MBP labeling was seen in large areas along the CC and cortex of nontreated animals during the recovery phase, which reflects irregular recovery of the OL population and myelin sheath formation after the HI insult. We also found that the iN administration of aTf enhanced the proliferation of OPCs in the CC and SVZ and protected these cells against apoptotic cell death after the HI incident.

In summary, our data suggest that the iN administration of aTf has the potential to be used for clinical treatment to protect OLs and neurons and to induce remyelination in demyelinating HI events. Our findings indicate aTf might be a potential inducer of myelinating OLs in the neonatal mouse brain in acute demyelination caused by HI. More important, this study shows that aTf, when iN administered, contributes to the differentiation/maturation of OLs and survival of subventricular zone progenitors after demyelination *in vivo*.

aTf Promotes OPC Maturation and Prevents Cell Death in Hypoxic Cultures

A major neuropathological feature of preterm HI brain injury is white matter damage, which manifests itself as periventricular leukomalacia and diffuse hypomyelination. White matter damage can result from early OPC loss and the failure of OPCs to differentiate into mature OLs (Back et al., 2007; Craig et al., 2003). OPCs predominate in the immature preterm brain between ~23 and 32 weeks gestation and are particularly susceptible to HI insults during this period (Back et al., 2001; 2007). Low levels of endogenous antioxidant enzymes in these early OPCs at least partly contribute to their demise (Back et al., 1998, 2007; Thorburne and Juurlink, 1996).

At present, our understanding of the influences of hypoxia on OPC development is limited. In this work we have used primary cultures of enriched OPCs to examine the isolated effects of hypoxia and aTf on OPC development. In agreement with our previous reports (Paez et al., 2002, 2004, 2005), we observed OPC maturation in the presence of aTf. A significant decrease in the proportion of NG2, Sox2, Sox9, and Olig2-positive cells was seen after exposure to aTf for 12 h under normal culture conditions. More importantly, under low oxygen concentration, the prodifferentiation effect of aTf was further enhanced. Additionally, we found a significant decrease in the number of apoptotic cells in OPC cultures subjected to hypoxia when aTf was present in the extracellular media, which suggests that aTf prevents OPC death by apoptosis. These observations are consistent with our *in vivo* findings of a reduction in the proportion of CNP-EGFP/caspase3 double positive cells in the brain of HI animals treated with aTf. The cellular basis of this observation is not clear. Yet, since we observe more mature forms of OLs in the presence of aTf than in its absence, it is possible that mature OLs are more tolerant to hypoxia than immature forms. In this line, Gerstner et al. (2009) have shown that OPCs are more sensitive to excitotoxic and oxidative injury than mature OLs (Back et al., 1998; Deng et al., 2003; Rosenberg et al., 2003) and that excitotoxicity plays a key role in a model of HI injury to developing white matter (Deng et al., 2004; Follett et al., 2000; Volpe, 2001).

In future studies, it will thus be important to quantify OL stage-specific subtypes in the brains of developing animals exposed to hypoxia and aTf, to determine whether our *in vitro* observations of premature OPC maturation are also seen *in vivo*. Overall, we find that aTf induces premature maturation of OPCs under hypoxic conditions. We postulate that premature maturation of OPCs will lead to an increase in the numbers of myelinating OLs in the brain. As such, premature OPC maturation induced by aTf may contribute to remyelination in the developing hypoxic brain.

ACKNOWLEDGMENTS

The authors thank Vittorio Gallo for kindly providing CNP-EGFP mice.

REFERENCES

Abercrombie M. 1946. Estimation of nuclear population from microtome sections. Anat Rec 94:239–247.

Adamo AM, Paez PM, Escobar Cabrera OE, Wolfson M, Franco PG, Pasquini JM, Soto EF. 2006. Remyelination after cuprizone-induced demyelination in the rat is stimulated by apotransferrin. Exp Neurol 198:519–529.

Agresti C, D'Urso D, Levi G. 1996. Reversible inhibitory effects of interferon-c and tumor necrosis factor-a on oligodendroglial lineage cell proliferation and differentiation in vitro. Eur J Neurosci 8:1106–1116.

Amur-Umarjee S, Phan T, Campagnoni AT. 1993. Myelin basic protein mRNA translocation in oligodendrocytes is inhibited by astrocytes in vitro. J Neurosci Res 36:99–110.

Back SA, Craig A, Luo NL, Ren J, Akundi RS, Ribeiro I, Rivkees SA. 2006. Protective effects of caffeine on chronic hypoxia-induced perinatal white matter injury. Ann Neurol 60:696–705.

Back SA, Gan X, Rosenberg PA, Volpe JJ. 1998. Maturation-dependent vulnerability of oligodendrocytes to oxidative stress-induced apoptosis caused by glutathione depletion. J Neurosci 18:6241–6253.

Back SA, Luo NL, Borenstein NS, Levine JM, Volpe JJ, Kinney HC. 2001. Late oligodendrocyte progenitors coincide with the developmental window of vulnerability for human perinatal white matter injury. J Neurosci 21:1302–1312.

Back SA, Riddle A, McClure MM. 2007. Maturation-dependent vulnerability of perinatal white matter in premature birth. Stroke 38(2 Suppl):724–730.

Badaracco ME, Ortiz EH, Soto EF, Pasquini JM. 2008. Effect of transferrin on hypomyelination induced by iron deficiency. J Neurosci Res 86:2663–2673.

Balin BJ, Broadwell RD, Salcman M, el-Kalliny M. 1986. Avenues for entry of peripherally administered protein to the central nervous system in mouse, rat, and squirrel monkey. J Comp Neurol 251:260–280.

Born J, Lange T, Kern W, McGregor GP, Bickel U, Fehm HL. 2002. Sniffing neuropeptides: A transnasal approach to the human brain. Nat Neurosci 5:514–516.

Cai Z, Lin S, Fan LW, Pang Y, Rhodes PG. 2006. Minocycline alleviates hypoxic-ischemic injury to developing oligodendrocytes in the neonatal rat brain. Neuroscience 137:425–435.

Carty ML, Wixey JA, Colditz PB, Buller KM. 2008. Post-insult minocycline treatment attenuates hypoxia-ischemia-induced neuroinflammation and white matter injury in the neonatal rat: A comparison of two different dose regimens. Int J Dev Neurosci 26:477–485.

Craig Andrew, Ning Ling Luo, Douglas JB, Nasiema W-P, David WW, Roger AH, Stephen B. 2003. Quantitative analysis of perinatal rodent oligodendrocyte lineage progression and its correlation with human. Exp Neurol 181:231–240.

Danielyan L, Schäfer R, von Ameln-Mayerhofer A, Bernhard F, Verleysdonk S, Buadze M, Lourhmati A, Klopfer T, Schaumann F, Schmid B, Koehle C, Proksch B, Weissert R, Reichardt HM, van den Brandt J, Buniatian GH, Schwab M, Gleiter CH, Frey WH II. 2011. Therapeutic efficacy of intranasally delivered mesenchymal stem cells in a rat model of Parkinson disease. Rejuvenation Res 14:3–16.

Danielyan L, Schäfer R, von Ameln-Mayerhofer A, Buadze M, Geisler J, Klopfer T, Burkhardt U, Proksch B, Verleysdonk S, Ayturan M, Buniatian GH, Gleiter CH, Frey WH II. 2009. Intranasal delivery of cells to the brain. Eur J Cell Biol 88:315–324.

Deng W, Rosenberg PA, Volpe JJ, Jensen FE. 2003. Calcium-permeable AMPA/kainate receptors mediate toxicity and preconditioning by oxygen-glucose deprivation in oligodendrocyte precursors. Proc Natl Acad Sci USA 100:6801–6806.

Deng W, Wang H, Rosenberg PA, Volpe JJ, Jensen FE. 2004. Role of metabotropic glutamate receptors in oligodendrocyte excitotoxicity and oxidative stress. Proc Natl Acad Sci USA 101:7751–7756.

Escobar Cabrera OE, Bongarzone ER, Soto EF, Pasquini JM. 1994. Single intracerebral injection of apotransferrin in young rats induces increased myelination. Dev Neurosci 16:248–254.

Escobar Cabrera OE, Soto EF, Pasquini JM. 2000. Myelin membranes isolated from rats intracranially injected with apotransferrin are more susceptible to in vitro peroxidation. Neurochem Res 25:87–93.

Escobar Cabrera OE, Zakin MM, Soto EF, Pasquini JM. 1997. Single intracranial injection of apotransferrin in young rats increases the expression of specific myelin protein mRNA. J Neurosci Res 47:603–608.

Espinosa de los Monteros A, Kumar S, Zhao P, Huang CJ, Nazarian R, Pan T, Scully S, Chang R, de Vellis J. 1999. Transferrin is an essential factor for myelination. Neurochem Res. 24:235–248.

Espinosa-Jeffrey A, Kumar S, Zhao PM, Awosika O, Agbo C, Huang A, Chang R, De Vellis J. 2002. Transferrin regulates transcription of the MBP gene and its action synergizes with IGF-1 to enhance myelinogenesis in the MD rat. Dev Neurosci 24:227–241.

Fan LW, Chen RF, Mitchell HJ, Lin RC, Simpson KL, Rhodes PG, Cai Z. 2008. Alpha-phenyl-*n*-tert-butyl-nitrone attenuates lipopolysaccharide-induced brain injury and improves neurological reflexes and early sensorimotor behavioral performance in juvenile rats. J Neurosci Res 86:3536–3547.

Fan LW, Lin S, Pang Y, Rhodes PG, Cai Z. 2006. Minocycline attenuates hypoxia-ischemia-induced neurological dysfunction and brain injury in the juvenile rat. Eur J Neurosci 24:341–350.

Ferriero DM, Holtzman DM, Black SM, Sheldon RA. 1996. Neonatal mice lacking neuronal nitric oxide synthase are less vulnerable to hypoxic-ischemic injury. Neurobiol Dis 3:64–71.

Follett PL, Rosenberg PA, Volpe JJ, Jensen FE. 2000. NBQX attenuates excitotoxic injury in developing white matter. J Neurosci 20:9235–9241.

Gerstner B, Lee J, DeSilva TM, Jensen FE, Volpe JJ, Rosenberg PA. 2009. 17beta-estradiol protects against hypoxic/ischemic white matter damage in the neonatal rat brain. J Neurosci Res 87:2078–2086.

Guan J, Skinner SJ, Beilharz EJ, Hua KM, Hodgkinson S, Gluckman PD, Williams CE. 1996. The movement of IGF-I into the brain parenchyma after hypoxic-ischaemic injury. Neuroreport 7:632–636.

Guardia Clausi M, Pasquini LA, Soto EF, Pasquini JM. 2010. Apotransferrin-induced recovery after hypoxic/ischaemic injury on myelination. ASN Neurol 2:e00048.

Han Y, Malak H, Chaudhary AG, Chordia MD, Kingston DG, Bane S. 1998. Distances between the paclitaxel, colchicine, and exchangeable GTP binding sites on tubulin. Biochemistry 37:6636–6644.

Hanson LR, Roeytenberg A, Martinez PM, Coppes VG, Sweet DC, Rao RJ, Marti DL, Hoekman JD, Matthews RB, Frey WH II, Panter SS. 2009. Intranasal deferoxamine provides increased brain exposure and significant protection in rat ischemic stroke. J Pharmacol Exp Ther 330:679–686.

Hastie SB. 1991. Interactions of colchicine with tubulin. Pharmacol Ther 51:377–401.

Illum L. 2004. Is nose-to-brain transport of drugs in man a reality? J Pharm Pharmacol 56:3–17.

Jung C, Chylinski TM, Pimenta A, Ortiz D, Shea TB. 2004. Neurofilament transport is dependent on actin and myosin. J Neurosci 24:9486–9496.

Liu XF, Fawcett JR, Thorne RG, DeFor TA, Frey WH II. 2001b. Intranasal administration of insulin-like growth factor-I bypasses the blood-brain barrier and protects against focal cerebral ischemic damage. J Neurol Sci 187:91–97.

Liu XF, Fawcett JR, Thorne RG, Frey WH II. 2001a. Non-invasive intranasal insulin-like growth factor-I reduces infarct volume and improves neurologic function in rats following middle cerebral artery occlusion. Neurosci Lett 308:91–94.

Marta CB, Paez P, Lopez M, Pellegrino de Iraldi A, Soto EF, Pasquini JM. 2003. Morphological changes of myelin sheaths in rats intracranially injected with apotransferrin. Neurochem Res 28:101–110.

Moos T, Bernth N, Courtois Y, Morgan EH. 2011. Developmental iron uptake and axonal transport in the retina of the rat. Mol Cell Neurosci 46:607–613.

Oh LY, Denninger A, Colvin JS, Vyas A, Tole S, Ornitz DM, Bansal R. 2003. Fibroblast growth factor receptor 3 signaling regulates the onset of oligodendrocyte terminal differentiation. J Neurosci 23:883–894.

Paez PM, Fulton DJ, Spreuer V, Handley V, Campagnoni CW, Campagnoni AT. 2009. Regulation of store-operated and voltage-operated Ca2+ channels in the proliferation and death of oligodendrocyte precursor cells by golli proteins. ASN Neurol 1:1–15.

Paez PM, García CI, Campagnoni AT, Soto EF, Pasquini JM. 2005. Overexpression of human transferrin in two oligodendroglial cell lines enhances their differentiation. Glia 52:1–15.

Paez PM, Garcia CI, Davio C, Campagnoni AT, Soto EF, Pasquini JM. 2004. Apotransferrin promotes the differentiation of two oligodendroglial cell lines. Glia 46:207–217.

Paez PM, Marta CB, Moreno MB, Soto EF, Pasquini JM. 2002. Apotransferrin decreases migration and enhances differentiation of oligodendroglial progenitor cells in an in vitro system. Dev Neurosci 24:47–58.

Reyes SD, Campagnoni AT. 2002. Two separate domains in the golli myelin basic proteins are responsible for nuclear targeting and process extension in transfected cells. J Neurosci Res 69:587–596.

Rice JE III, Vannucci RC, Brierley JB. 1981. The influence of immaturity on hypoxic-ischemic brain damage in the rat. Ann Neurol 9:131–141.

Rosenberg PA, Dai W, Gan XD, Ali S, Fu J, Back SA, Sanchez RM, Segal MM, Follett PL, Jensen FE, Volpe JJ. 2003. Mature myelin basic protein-expressing oligodendrocytes are insensitive to kainate toxicity. J Neurosci Res 71:237–245.

Saleh MC, Espinosa de los Monteros A, de Arriba Zerpa GA, Fontaine I, Piaud O, Djordjijevic D, Baroukh N, Garcia Otin AL, Ortiz E, Lewis S, Fiette L, Santambrogio P, Belzung C, Connor JR, de Vellis J, Pasquini JM, Zakin MM, Baron B, Guillou F. 2003. Myelination and motor coordination are increased in transferrin transgenic mice. J Neurosci Res 72:587–594.

Suzumura A, Bhat S, Eccleston PA, Lisak RP, Silberberg DH. 1984. The isolation and long-term culture of oligodendrocytes from newborn mouse brain. Brain Res 324:379–383.

Thorne RG, Emory CR, Ala TA, Frey WH II. 1995. Quantitative analysis of the olfactory pathway for drug delivery to the brain. Brain Res 692:278–282.

Thorne RG, Frey WH II. 2001. Delivery of neurotrophic factors to the central nervous system: Pharmacokinetic considerations. Clin Pharmacokinet 40:907–946.

Thorburne SK, Juurlink BH. 1996. Low glutathione and high iron govern the susceptibility of oligodendroglial precursors to oxidative stress. J Neurochem 67:1014–1022.

Volpe JJ. 2001. Neurobiology of periventricular leukomalacia in the premature infant. Pediatr Res 50:553–562.

Wood TL, Loladze V, Altieri S, Gangoli N, Levison SW, Brywe KG, Mallard C, Hagberg H. 2007. Delayed IGF-1 administration rescues oligodendrocyte progenitors from glutamate-induced cell death and hypoxic-ischemic brain damage. Dev Neurosci 9:302–310.

Yang JP, Liu HJ, Wang ZL, Cheng SM, Cheng X, Xu GL, Liu XF. 2009. The dose-effectiveness of intranasal VEGF in treatment of experimental stroke. Neurosci Lett 461:212–216.

Yuan X, Chittajallu R, Belachew S, Anderson S, McBain CJ, Gallo V. 2002. Expression of the green fluorescent protein in the oligodendrocyte lineage: A transgenic mouse for developmental and physiological studies. J Neurosci Res 70:529–545.

Yuko Y, Narito T, Taiji S, Souichi S, Eriko O, Setsuya F. 2004. Relationship between S100h and GFAP expression in astrocytes during infarction and glial scar formation after mild transient ischemia. Brain Res 1021:20–31.